

DESY-11-005

19 January 2011

Measurement of beauty production in deep inelastic scattering at HERA using decays into electrons

ZEUS Collaboration

Abstract

The production of beauty quarks in ep interactions has been studied with the ZEUS detector at HERA for exchanged four-momentum squared $Q^2 > 10 \text{ GeV}^2$, using an integrated luminosity of 363 pb^{-1} . The beauty events were identified using electrons from semileptonic b decays with a transverse momentum $0.9 < p_T^e < 8 \text{ GeV}$ and pseudorapidity $|\eta^e| < 1.5$. Cross sections for beauty production were measured and compared with next-to-leading-order QCD calculations. The beauty contribution to the proton structure function F_2 was extracted from the double-differential cross section as a function of Bjorken- x and Q^2 .

The ZEUS Collaboration

H. Abramowicz^{45,ah}, I. Abt³⁵, L. Adamczyk¹³, M. Adamus⁵⁴, R. Aggarwal^{7,d}, S. Antonelli⁴, P. Antonioli³, A. Antonov³³, M. Arneodo⁵⁰, V. Aushev^{26,27,aa}, Y. Aushev^{27,aa,ab}, O. Bachynska¹⁵, A. Bamberger¹⁹, A.N. Barakbaev²⁵, G. Barbagli¹⁷, G. Bari³, F. Barreiro³⁰, N. Bartosik^{27,ac}, D. Bartsch⁵, M. Basile⁴, O. Behnke¹⁵, J. Behr¹⁵, U. Behrens¹⁵, L. Bellagamba³, A. Bertolin³⁹, S. Bhadra⁵⁷, M. Bindi⁴, C. Blohm¹⁵, V. Bokhonov^{26,aa}, T. Bołd¹³, O. Bolilyi^{27,ac}, E.G. Boos²⁵, K. Borras¹⁵, D. Boscherini³, D. Bot¹⁵, S.K. Boutle⁵², I. Brock⁵, E. Brownson⁵⁶, R. Brugnera⁴⁰, N. Brümmer³⁷, A. Bruni³, G. Bruni³, B. Brzozowska⁵³, P.J. Bussey²⁰, J.M. Butterworth⁵², B. Bylsma³⁷, A. Caldwell³⁵, M. Capua⁸, R. Carlin⁴⁰, C.D. Catterall⁵⁷, S. Chekanov¹, J. Chwastowski^{12,f}, J. Ciborowski^{53,al}, R. Ciesielski^{15,h}, L. Cifarelli⁴, F. Cindolo³, A. Contin⁴, A.M. Cooper-Sarkar³⁸, N. Coppola^{15,i}, M. Corradi³, F. Corriveau³¹, M. Costa⁴⁹, G. D'Agostini⁴³, F. Dal Corso³⁹, J. del Peso³⁰, R.K. Dementiev³⁴, S. De Pasquale^{4,b}, M. Derrick¹, R.C.E. Devenish³⁸, D. Dobur^{19,u}, B.A. Dolgoshein^{33,†}, G. Dolinska^{26,27}, A.T. Doyle²⁰, V. Drugakov¹⁶, L.S. Durkin³⁷, S. Dusini³⁹, Y. Eisenberg⁵⁵, P.F. Ermolov^{34,†}, A. Eskreys¹², S. Fang^{15,j}, S. Fazio⁸, J. Ferrando³⁸, M.I. Ferrero⁴⁹, J. Figiel¹², M. Forrest²⁰, B. Foster³⁸, S. Fourletov^{51,w}, G. Gach¹³, A. Galas¹², E. Gallo¹⁷, A. Garfagnini⁴⁰, A. Geiser¹⁵, I. Gialas^{21,x}, L.K. Gladilin³⁴, D. Gladkov³³, C. Glasman³⁰, O. Gogota^{26,27}, Yu.A. Golubkov³⁴, P. Göttlicher^{15,k}, I. Grabowska-Bołd¹³, J. Grebenyuk¹⁵, I. Gregor¹⁵, G. Grigorescu³⁶, G. Grzelak⁵³, O. Gueta⁴⁵, C. Gwenlan^{38,ae}, T. Haas¹⁵, W. Hain¹⁵, R. Hamatsu⁴⁸, J.C. Hart⁴⁴, H. Hartmann⁵, G. Hartner⁵⁷, E. Hilger⁵, D. Hochman⁵⁵, R. Hori⁴⁷, K. Horton^{38,af}, A. Hüttmann¹⁵, G. Iacobucci³, Z.A. Ibrahim¹⁰, Y. Iga⁴², R. Ingbir⁴⁵, M. Ishitsuka⁴⁶, H.-P. Jakob⁵, F. Januschek¹⁵, M. Jimenez³⁰, T.W. Jones⁵², M. Jüngst⁵, I. Kadenko²⁷, B. Kahle¹⁵, B. Kamaluddin^{10,†}, S. Kananov⁴⁵, T. Kanno⁴⁶, U. Karshon⁵⁵, F. Karstens^{19,v}, I.I. Katkov^{15,l}, M. Kaur⁷, P. Kaur^{7,d}, A. Keramidis³⁶, L.A. Khein³⁴, J.Y. Kim⁹, D. Kisielewska¹³, S. Kitamura^{48,aj}, R. Klanner²², U. Klein^{15,m}, E. Koffeman³⁶, P. Kooijman³⁶, Ie. Korol^{26,27}, I.A. Korzhavina³⁴, A. Kotański^{14,g}, U. Kötz¹⁵, H. Kowalski¹⁵, P. Kulinski⁵³, O. Kuprash^{27,ad}, M. Kuze⁴⁶, A. Lee³⁷, B.B. Levchenko³⁴, A. Levy⁴⁵, V. Libov¹⁵, S. Limentani⁴⁰, T.Y. Ling³⁷, M. Lisovyi¹⁵, E. Lobodzinska¹⁵, W. Lohmann¹⁶, B. Lühr¹⁵, E. Lohrmann²², J.H. Loizides⁵², K.R. Long²³, A. Longhin³⁹, D. Lontkovskiy^{27,ad}, O.Yu. Lukina³⁴, P. Łuźniak^{53,am}, J. Maeda^{46,ai}, S. Magill¹, I. Makarenko^{27,ad}, J. Malka^{53,am}, R. Mankel¹⁵, A. Margotti³, G. Marini⁴³, J.F. Martin⁵¹, A. Mastroberardino⁸, M.C.K. Mattingly², I.-A. Melzer-Pellmann¹⁵, S. Mergelmeyer⁵, S. Miglioranzi^{15,n}, F. Mohamad Idris¹⁰, V. Monaco⁴⁹, A. Montanari¹⁵, J.D. Morris^{6,c}, K. Mujkic^{15,o}, B. Musgrave¹, K. Nagano²⁴, T. Namsoo^{15,p}, R. Nania³, D. Nicholass^{1,a}, A. Nigro⁴³, Y. Ning¹¹, U. Noor⁵⁷, D. Notz¹⁵, R.J. Nowak⁵³, A.E. Nuncio-Quiroz⁵, B.Y. Oh⁴¹, N. Okazaki⁴⁷, K. Oliver³⁸, K. Olkiewicz¹², Yu. Onishchuk²⁷, K. Papageorgiu²¹, A. Parenti¹⁵, E. Paul⁵, J.M. Pawlak⁵³, B. Pawlik¹², P. G. Pelfer¹⁸, A. Pellegrino³⁶, W. Perlanski^{53,am}, H. Perrey²², K. Piotrkowski²⁹, P. Plucinski^{54,an}, N.S. Pokrovskiy²⁵, A. Polini³, A.S. Proskuryakov³⁴, M. Przybycień¹³, A. Raval¹⁵, D.D. Reeder⁵⁶, B. Reisert³⁵, Z. Ren¹¹, J. Repond¹, Y.D. Ri^{48,ak}, A. Robertson³⁸, P. Roloff¹⁵, E. Ron³⁰, I. Rubinsky¹⁵, M. Ruspa⁵⁰, R. Sacchi⁴⁹, A. Saliı̄²⁷, U. Samson⁵, G. Sartorelli⁴, A.A. Savin⁵⁶, D.H. Saxon²⁰, M. Schioppa⁸, S. Schlenstedt¹⁶, P. Schleper²², W.B. Schmidke³⁵, U. Schneekloth¹⁵, V. Schönberg⁵, T. Schörner-Sadenius¹⁵, J. Schwartz³¹,

F. Sciulli¹¹, L.M. Shcheglova³⁴, R. Shehzadi⁵, S. Shimizu^{47,n}, I. Singh^{7,d}, I.O. Skillicorn²⁰, W. Słomiński¹⁴, W.H. Smith⁵⁶, V. Sola⁴⁹, A. Solano⁴⁹, D. Son²⁸, V. Sosnovtsev³³, A. Spiridonov^{15,q}, H. Stadie²², L. Stanco³⁹, A. Stern⁴⁵, T.P. Stewart⁵¹, A. Stifutkin³³, P. Stopa¹², S. Suchkov³³, G. Susinno⁸, L. Suszycki¹³, J. Sztuk-Dambietz²², D. Szuba^{15,r}, J. Szuba^{15,s}, A.D. Tapper²³, E. Tassi^{8,e}, J. Terrón³⁰, T. Theedt¹⁵, H. Tiecke³⁶, K. Tokushuku^{24,y}, O. Tomalak²⁷, J. Tomaszewska^{15,t}, T. Tsurugai³², M. Turcato²², T. Tymieniecka^{54,ao}, C. Uribe-Estrada³⁰, M. Vázquez^{36,n}, A. Verbytskyi¹⁵, O. Viazlo^{26,27}, N.N. Vlasov^{19,w}, O. Volynets²⁷, R. Walczak³⁸, W.A.T. Wan Abdullah¹⁰, J.J. Whitmore^{41,ag}, J. Whyte⁵⁷, L. Wiggers³⁶, M. Wing⁵², M. Wlasenko⁵, G. Wolf¹⁵, H. Wolfe⁵⁶, K. Wrona¹⁵, A.G. Yagües-Molina¹⁵, S. Yamada²⁴, Y. Yamazaki^{24,z}, R. Yoshida¹, C. Youngman¹⁵, A.F. Żarnecki⁵³, L. Zawiejski¹², O. Zenaiev²⁷, W. Zeuner^{15,n}, B.O. Zhautykov²⁵, N. Zhmak^{26,aa}, C. Zhou³¹, A. Zichichi⁴, M. Zolko²⁷, D.S. Zotkin³⁴, Z. Zulkapli¹⁰

- 1 *Argonne National Laboratory, Argonne, Illinois 60439-4815, USA*^A
2 *Andrews University, Berrien Springs, Michigan 49104-0380, USA*
3 *INFN Bologna, Bologna, Italy*^B
4 *University and INFN Bologna, Bologna, Italy*^B
5 *Physikalisches Institut der Universität Bonn, Bonn, Germany*^C
6 *H.H. Wills Physics Laboratory, University of Bristol, Bristol, United Kingdom*^D
7 *Panjab University, Department of Physics, Chandigarh, India*
8 *Calabria University, Physics Department and INFN, Cosenza, Italy*^B
9 *Institute for Universe and Elementary Particles, Chonnam National University,*
10 *Kwangju, South Korea*
11 *Jabatan Fizik, Universiti Malaya, 50603 Kuala Lumpur, Malaysia*^E
12 *Nevis Laboratories, Columbia University, Irvington on Hudson, New York 10027,*
13 *USA*^F
14 *The Henryk Niewodniczanski Institute of Nuclear Physics, Polish Academy of*
15 *Sciences, Cracow, Poland*^G
16 *Faculty of Physics and Applied Computer Science, AGH-University of Science and*
17 *Technology, Cracow, Poland*^H
18 *Department of Physics, Jagellonian University, Cracow, Poland*
19 *Deutsches Elektronen-Synchrotron DESY, Hamburg, Germany*
20 *Deutsches Elektronen-Synchrotron DESY, Zeuthen, Germany*
21 *INFN Florence, Florence, Italy*^B
22 *University and INFN Florence, Florence, Italy*^B
23 *Fakultät für Physik der Universität Freiburg i.Br., Freiburg i.Br., Germany*
24 *School of Physics and Astronomy, University of Glasgow, Glasgow, United King-*
25 *dom*^D
26 *Department of Engineering in Management and Finance, Univ. of the Aegean,*
27 *Chios, Greece*
28 *Hamburg University, Institute of Experimental Physics, Hamburg, Germany*^I
29 *Imperial College London, High Energy Nuclear Physics Group, London, United*
30 *Kingdom*^D
31 *Institute of Particle and Nuclear Studies, KEK, Tsukuba, Japan*^J
32 *Institute of Physics and Technology of Ministry of Education and Science of Kaza-*
khstan, Almaty, Kazakhstan
33 *Institute for Nuclear Research, National Academy of Sciences, Kyiv, Ukraine*
34 *Department of Nuclear Physics, National Taras Shevchenko University of Kyiv,*
35 *Kyiv, Ukraine*
36 *Kyungpook National University, Center for High Energy Physics, Daegu, South Ko-*
37 *rea*^K
38 *Institut de Physique Nucléaire, Université Catholique de Louvain, Louvain-la-Neuve,*
39 *Belgium*^L
40 *Departamento de Física Teórica, Universidad Autónoma de Madrid, Madrid,*
41 *Spain*^M
42 *Department of Physics, McGill University, Montréal, Québec, Canada H3A 2T8*^N
43 *Meiji Gakuin University, Faculty of General Education, Yokohama, Japan*^J

- 33 *Moscow Engineering Physics Institute, Moscow, Russia*^O
34 *Moscow State University, Institute of Nuclear Physics, Moscow, Russia*^P
35 *Max-Planck-Institut für Physik, München, Germany*
36 *NIKHEF and University of Amsterdam, Amsterdam, Netherlands*^Q
37 *Physics Department, Ohio State University, Columbus, Ohio 43210, USA*^A
38 *Department of Physics, University of Oxford, Oxford, United Kingdom*^D
39 *INFN Padova, Padova, Italy*^B
40 *Dipartimento di Fisica dell' Università and INFN, Padova, Italy*^B
41 *Department of Physics, Pennsylvania State University, University Park,
Pennsylvania 16802, USA*^F
42 *Polytechnic University, Sagamihara, Japan*^J
43 *Dipartimento di Fisica, Università 'La Sapienza' and INFN, Rome, Italy*^B
44 *Rutherford Appleton Laboratory, Chilton, Didcot, Oxon, United Kingdom*^D
45 *Raymond and Beverly Sackler Faculty of Exact Sciences, School of Physics,
Tel Aviv University, Tel Aviv, Israel*^R
46 *Department of Physics, Tokyo Institute of Technology, Tokyo, Japan*^J
47 *Department of Physics, University of Tokyo, Tokyo, Japan*^J
48 *Tokyo Metropolitan University, Department of Physics, Tokyo, Japan*^J
49 *Università di Torino and INFN, Torino, Italy*^B
50 *Università del Piemonte Orientale, Novara, and INFN, Torino, Italy*^B
51 *Department of Physics, University of Toronto, Toronto, Ontario, Canada M5S
1A7*^N
52 *Physics and Astronomy Department, University College London, London, United
Kingdom*^D
53 *Faculty of Physics, University of Warsaw, Warsaw, Poland*
54 *Institute for Nuclear Studies, Warsaw, Poland*
55 *Department of Particle Physics and Astrophysics, Weizmann Institute, Rehovot,
Israel*
56 *Department of Physics, University of Wisconsin, Madison, Wisconsin 53706, USA*^A
57 *Department of Physics, York University, Ontario, Canada M3J 1P3*^N

- A* supported by the US Department of Energy
- B* supported by the Italian National Institute for Nuclear Physics (INFN)
- C* supported by the German Federal Ministry for Education and Research (BMBF),
under contract No. 05 H09PDF
- D* supported by the Science and Technology Facilities Council, UK
- E* supported by an FRGS grant from the Malaysian government
- F* supported by the US National Science Foundation. Any opinion, findings and conclusions or recommendations expressed in this material are those of the authors and do not necessarily reflect the views of the National Science Foundation.
- G* supported by the Polish Ministry of Science and Higher Education as a scientific project No. DPN/N188/DESY/2009
- H* supported by the Polish Ministry of Science and Higher Education as a scientific project (2009-2010)
- I* supported by the German Federal Ministry for Education and Research (BMBF),
under contract No. 05h09GUF, and the SFB 676 of the Deutsche Forschungsgemeinschaft (DFG)
- J* supported by the Japanese Ministry of Education, Culture, Sports, Science and Technology (MEXT) and its grants for Scientific Research
- K* supported by the Korean Ministry of Education and Korea Science and Engineering Foundation
- L* supported by FNRS and its associated funds (IISN and FRIA) and by an Inter-University Attraction Poles Programme subsidised by the Belgian Federal Science Policy Office
- M* supported by the Spanish Ministry of Education and Science through funds provided by CICYT
- N* supported by the Natural Sciences and Engineering Research Council of Canada (NSERC)
- O* partially supported by the German Federal Ministry for Education and Research (BMBF)
- P* supported by RF Presidential grant N 41-42.2010.2 for the Leading Scientific Schools and by the Russian Ministry of Education and Science through its grant for Scientific Research on High Energy Physics
- Q* supported by the Netherlands Foundation for Research on Matter (FOM)
- R* supported by the Israel Science Foundation

- a* also affiliated with University College London, United Kingdom
- b* now at University of Salerno, Italy
- c* now at Queen Mary University of London, United Kingdom
- d* also funded by Max Planck Institute for Physics, Munich, Germany
- e* also Senior Alexander von Humboldt Research Fellow at Hamburg University, Institute of Experimental Physics, Hamburg, Germany
- f* also at Cracow University of Technology, Faculty of Physics, Mathematics and Applied Computer Science, Poland
- g* supported by the research grant No. 1 P03B 04529 (2005-2008)
- h* now at Rockefeller University, New York, NY 10065, USA
- i* now at DESY group FS-CFEL-1
- j* now at Institute of High Energy Physics, Beijing, China
- k* now at DESY group FEB, Hamburg, Germany
- l* also at Moscow State University, Russia
- m* now at University of Liverpool, United Kingdom
- n* now at CERN, Geneva, Switzerland
- o* also affiliated with Universtiy College London, UK
- p* now at Goldman Sachs, London, UK
- q* also at Institute of Theoretical and Experimental Physics, Moscow, Russia
- r* also at INP, Cracow, Poland
- s* also at FPACS, AGH-UST, Cracow, Poland
- t* partially supported by Warsaw University, Poland
- u* now at Istituto Nucleare di Fisica Nazionale (INFN), Pisa, Italy
- v* now at Haase Energie Technik AG, Neumünster, Germany
- w* now at Department of Physics, University of Bonn, Germany
- x* also affiliated with DESY, Germany
- y* also at University of Tokyo, Japan
- z* now at Kobe University, Japan
- † deceased
- aa* supported by DESY, Germany
- ab* member of National Technical University of Ukraine, Kyiv Polytechnic Institute, Kyiv, Ukraine
- ac* member of National University of Kyiv - Mohyla Academy, Kyiv, Ukraine
- ad* supported by the Bogolyubov Institute for Theoretical Physics of the National Academy of Sciences, Ukraine
- ae* STFC Advanced Fellow
- af* nee Korcsak-Gorzo
- ag* This material was based on work supported by the National Science Foundation, while working at the Foundation.
- ah* also at Max Planck Institute for Physics, Munich, Germany, External Scientific Member
- ai* now at Tokyo Metropolitan University, Japan
- aj* now at Nihon Institute of Medical Science, Japan

- ak* now at Osaka University, Osaka, Japan
- al* also at Łódź University, Poland
- am* member of Łódź University, Poland
- an* now at Lund University, Lund, Sweden
- ao* also at University of Podlasie, Siedlce, Poland

1 Introduction

The production of heavy quarks in ep collisions at HERA is an important testing ground for perturbative Quantum Chromodynamics (pQCD), since the large b -quark mass provides a hard scale that allows perturbative calculations to be made [1,2]. The dominant production process is boson-gluon fusion (BGF) between the incoming virtual photon and a gluon in the proton. Beauty production has been measured using several methods by the ZEUS [3–11] and the H1 [12–18] collaborations both in deep inelastic scattering (DIS), i.e. for large exchanged four-momentum squared, Q^2 , and also in photoproduction, i.e. for $Q^2 \sim 0 \text{ GeV}^2$. The measurements are reasonably well described by next-to-leading-order (NLO) QCD predictions.

Most of the previous measurements of b -quark production used muons to tag semileptonic decays of the B hadrons. This paper reports a measurement of beauty production in DIS using the semileptonic decays to electrons,

$$ep \rightarrow e' b\bar{b} X \rightarrow e' e X',$$

in the kinematic range $Q^2 > 10 \text{ GeV}^2$. Using the electron channel allows a measurement of the decay leptons at lower transverse momentum and provides a complementary measurement, with independent systematics.

An analysis of the same process in the photoproduction regime, based on data taken in 1996–2000 (120 pb^{-1}), used a likelihood-ratio test to extract the signal of beauty and charm semileptonic decays to electrons [7]. A similar method, adapted to the different kinematics of the DIS regime, was used for the measurement reported here. The analysis also benefited from improved tracking in the more recent data, which allowed the measured decay length of weakly decaying B hadrons to be used.

In this analysis, the total visible cross section, $\sigma_{b \rightarrow e}$, and differential cross sections as a function of Q^2 , the Bjorken scaling variable, x , the transverse momentum, p_T^e , and the pseudorapidity of the electron, η^e , were measured. They are compared to a leading-order (LO) plus parton-shower (PS) Monte Carlo prediction and to an NLO QCD calculation. The beauty contribution to the proton structure function F_2 , denoted as $F_2^{b\bar{b}}$, was extracted from the double-differential cross section as a function of Q^2 and x and is compared with theoretical calculations.

2 Experimental set-up

This analysis was performed with data taken from 2004 to 2007, when HERA collided electrons or positrons with energy $E_e = 27.5 \text{ GeV}$ with protons of an energy of 920 GeV ,

corresponding to a centre-of-mass energy $\sqrt{s} = 318 \text{ GeV}$. This data-taking period is denoted as HERA II. The corresponding integrated luminosity is $(363 \pm 7) \text{ pb}^{-1}$.

A detailed description of the ZEUS detector can be found elsewhere [19]. A brief outline of the components that are most relevant for this analysis is given below.

In the kinematic range of the analysis, charged particles were tracked in the central tracking detector (CTD) [20] and the microvertex detector (MVD) [21]. These components operated in a magnetic field of 1.43 T provided by a thin superconducting solenoid. The CTD consisted of 72 cylindrical drift chamber layers, organised in nine superlayers covering the polar-angle¹ region $15^\circ < \theta < 164^\circ$. The MVD silicon tracker consisted of a barrel (BMVD) and a forward (FMVD) section. The BMVD provided polar-angle coverage for tracks with three measurements from 30° to 150° . The FMVD extended the polar-angle coverage in the forward region to 7° . After alignment, the single-hit resolution of the BMVD was $24 \mu\text{m}$ and the average impact parameter resolution of the CTD-BMVD system for high-momentum tracks was $100 \mu\text{m}$.

To estimate the ionisation energy loss per unit length, dE/dx , of particles in the CTD [22], the truncated mean of the anode-wire pulse heights was calculated, which removes the lowest 10% and at least the highest 30% depending on the number of saturated hits. The measured dE/dx values were corrected by normalising to the average dE/dx for tracks around the region of minimum ionisation for pions with momentum, p , satisfying $0.3 < p < 0.4 \text{ GeV}$ [23].

The high-resolution uranium–scintillator calorimeter (CAL) [24] consisted of three parts: the forward (FCAL), the barrel (BCAL) and the rear (RCAL) calorimeters. Each part was subdivided transversely into towers and longitudinally into one electromagnetic section and either one (in RCAL) or two (in BCAL and FCAL) hadronic sections. The smallest subdivision of the calorimeter is called a cell. The CAL energy resolutions, as measured under test-beam conditions, are $\sigma(E)/E = 0.18/\sqrt{E}$ for electrons and $\sigma(E)/E = 0.35/\sqrt{E}$ for hadrons, with E in GeV.

The luminosity was measured using the Bethe-Heitler reaction $ep \rightarrow e\gamma p$ by a luminosity detector which consisted of independent lead–scintillator calorimeter [25] and magnetic spectrometer [26] systems.

¹The ZEUS coordinate system is a right-handed Cartesian system, with the Z axis pointing in the proton beam direction, referred to as the “forward direction”, and the X axis pointing left towards the centre of HERA. The coordinate origin is at the nominal interaction point. The pseudorapidity is defined as $\eta = -\ln(\tan \frac{\theta}{2})$, where the polar angle, θ , is measured with respect to the proton beam direction. The azimuthal angle, ϕ , is measured with respect to the X axis.

3 Monte Carlo simulation

To evaluate the detector acceptance and to provide the signal and background distributions for the likelihood-ratio test, Monte Carlo (MC) samples of beauty, charm and light-flavour events were generated, corresponding to eighteen, two and one times the integrated luminosity of the data, respectively. The RAPGAP 3.00 Monte Carlo program [27] was used to generate the beauty and charm samples. The CTEQ5L [28] parton density functions were used and the heavy-quark masses were set to $m_b = 4.75$ GeV and $m_c = 1.5$ GeV. To simulate radiative corrections, the events were passed through the HERACLES 4.6 [29] program. An inclusive MC sample containing all flavours was generated using DJANGO 1.6 [30] interfaced to ARIADNE 4.12 [31], where the quarks were taken to be massless. The CTEQ5D [28] parton density functions were used.

For the acceptance determination, the Q^2 distribution in the signal MC was reweighted in order to correct for observed differences between the measured and simulated distributions. The corrections varied from +10% at low Q^2 to -30% at high Q^2 . The B -hadron lifetimes were corrected for differences between the simulated values and the world-average values [32].

Fragmentation and particle decays were simulated using the JETSET/PYTHIA model [33]. The lepton energy spectrum from charm decays was reweighted to agree with CLEO data [34]. The generated events were passed through a full simulation of the ZEUS detector based on GEANT 3.21 [35]. The final MC events had to fulfil the same trigger requirements and pass the same reconstruction program as the data.

4 Theoretical predictions and uncertainties

Next-to-leading-order QCD predictions were obtained from the HVQDIS [36] program in the fixed-flavour-number scheme (FFNS) [37]. More details about the calculation can be found elsewhere [4].

The b -quark mass (pole mass) was set to $m_b = 4.75$ GeV. The renormalisation and factorisation scales, μ_R and μ_F , were chosen to be equal and set to $\mu_R = \mu_F = \sqrt{Q^2 + 4m_b^2}$. The parton density functions were obtained from the FFNS variant of the ZEUS-S fit [38] using the same b -quark mass as in the HVQDIS calculation. The value of $\alpha_s(M_Z)$ was set to 0.105.

The Peterson fragmentation function [39], with $\epsilon_b = 0.0035$ [40], was used to produce beauty hadrons from the heavy quarks. The semileptonic decay spectrum was taken from the PYTHIA Monte Carlo. The contributions from prompt and from cascade decays,

$b \rightarrow c(\bar{c}) \rightarrow e$, including $b \rightarrow \tau \rightarrow e$ and $b \rightarrow J/\psi \rightarrow e^+e^-$, were taken into account in the effective branching fraction, which was set to 0.217 [32].

To estimate the uncertainty on the theoretical predictions, the b -quark mass was varied in the range $m_b = 4.5, 5.0$ GeV, and the scales μ_R, μ_F were varied independently by a factor of two up and down. The parameter ϵ_b was varied by ± 0.002 . The parton density functions were varied within the total uncertainties of the fit. The uncertainty on the NLO QCD prediction for the total cross section is +15% and -16%, where the dominant contribution originates from the variation of the mass and the scales.

The HVQDIS calculations were also used to extrapolate the visible cross sections to $F_2^{b\bar{b}}$.

5 Data selection

Events were selected online with a three-level trigger [19, 41] using a combination of triggers, which required a scattered electron to be detected in the CAL and/or the presence of an electron candidate from a semileptonic decay. Further details on the trigger chain can be found elsewhere [42]. Offline, the reconstructed scattered electron was required to have an energy $E_{e'} > 10$ GeV. The Z position of the primary vertex had to be within $|Z_{\text{vtx}}| < 30$ cm.

The final state of the electron-proton collision, including the scattered electron, was reconstructed from energy-flow objects (EFOs) [43] which combine the information from calorimetry and tracking, corrected for the energy loss in the detector material. Each EFO was assigned a reconstructed four-momentum, $q^i = (p_X^i, p_Y^i, p_Z^i, E^i)$. Jets were reconstructed from EFOs using the k_T algorithm [44] in the longitudinally invariant mode with the massive recombination scheme [45].

The following cuts were applied to select DIS events:

- the photon virtuality, Q^2 , must be above 10 GeV², where this variable and Bjorken- x were reconstructed using the double-angle method [46];
- $0.05 < y < 0.7$, where the inelasticity, y , was reconstructed using the Jacquet-Blondel method [47] for the lower cut and the electron method [46] for the higher cut;
- $40 < (E - p_Z)_{\text{tot}} < 65$ GeV, reconstructed using the four-momentum of the final state; this selects fully contained neutral-current electron-proton events for which $E - p_Z = 2 \cdot E_e = 55$ GeV;
- $P_T/E_T < 0.7$, where P_T and E_T are the transverse momentum and the scalar transverse energy of the final state. This cut was applied to reduce the charged-current and non- ep backgrounds.

In order to estimate the decay length of the B hadron, a secondary vertex was fitted using all good tracks assigned to the jet [48]. Good tracks were defined by a minimal transverse momentum, $p_T > 0.5 \text{ GeV}$, at least four hits in the MVD and three or more superlayers passed in the CTD. Vertices with $\chi^2/\text{dof} < 6$ and a distance from the interaction point within $\pm 1 \text{ cm}$ in the X - Y plane and $\pm 30 \text{ cm}$ in the Z direction were taken.

The decay length, d , was defined as the distance in XY between the secondary vertex and the interaction point², projected onto the jet axis. The sign of the decay length was assigned using the axis of the jet to which the vertex was associated; if the decay length vector was in the same hemisphere as the jet axis, a positive sign was assigned to it, otherwise the sign of the decay length was negative. Negative decay lengths, which originate from secondary vertices reconstructed on the wrong side of the interaction point with respect to the direction of the associated jets, are unphysical and caused by detector resolution effects. A small correction [42] to the MC decay-length distribution was applied in order to reproduce the data with negative values of decay length; 5% of the tracks in the central region were smeared and an additional smearing to tracks in the tails of the decay-length distribution was applied.

Electron candidates from semileptonic decays of b quarks were selected from the EFOs having a transverse momentum, p_T^e , satisfying $0.9 < p_T^e < 8 \text{ GeV}$ in the pseudorapidity range $|\eta^e| < 1.5$, and consisting of a track matched to a single calorimetric cluster. To reduce the hadronic background, at least 95% of the EFO energy had to be deposited in the electromagnetic part of the calorimeter. Candidates in the angular regions corresponding to the gaps between FCAL and BCAL as well as between RCAL and BCAL were removed. To account for differences in the η^e distribution in data and MC, the electron reconstruction efficiency in MC was corrected by 0.95 in the FCAL and RCAL regions and by 1.05 in the BCAL region. Electrons from identified photon conversions were rejected [11].

The electron candidate was required to be associated with a jet using the following criteria:

- the jet was required to have a reconstructed vertex of good quality as defined above;
- the jet had to have $p_T^{\text{jet}} > 2.5 \text{ GeV}$ and $|\eta^{\text{jet}}| < 2.0$;
- the distance $\Delta R = \sqrt{(\eta^{\text{jet}} - \eta^e)^2 + (\phi^{\text{jet}} - \phi^e)^2} < 1.0$;
- if there is more than one candidate jet, the jet closest in ΔR to the electron candidate was chosen.

² In the X - Y plane, the interaction point is defined as the centre of the beam ellipse, determined using the average primary vertex position for groups of a few thousand events, taking into account the difference in angle between the beam direction and the Z direction. The Z coordinate is taken as the Z position of the primary vertex of the event.

The combination of the momentum cut and the jet association reduces substantially the background from scattered electrons not identified as such.

The main variable for the electron identification was dE/dx [7]. To reduce the major background of fake electrons in the candidate selection, a preselection cut was applied on a likelihood-ratio test function $T_e^{dE/dx}$ [49]. This function was calculated using dE/dx as discriminating input variable and testing the electron hypothesis. The distribution of this test function, as obtained from MC, for the particle types e^\pm , π^\pm , p/\bar{p} and K^\pm is shown in Fig. 1. The vertical line at $-2 \ln T_e^{dE/dx} = 3$ indicates the cut, which rejects a large fraction of the background particles.

6 Identification of electrons from semileptonic decays

The electron candidates in the MC samples were classified into three different categories. The first category ($b \rightarrow e$) contains electrons from beauty decays, including direct semileptonic decays, cascade decays $b \rightarrow c(\bar{c}) \rightarrow e$, $b \rightarrow \tau \rightarrow e$ and $b \rightarrow J/\psi \rightarrow e^+e^-$. The second category (other e) contains all true electrons, which are not included in the beauty signal. These are mainly electrons originating from photon conversions, Dalitz decays, electrons from direct charm decays, or remaining DIS electrons. The third category (non- e) includes all candidates which are fake electrons. After the selection, the dominant contribution to the latter comes from pions, while the number of kaons or protons mimicking electrons is rather small.

For the electron identification, the following three variables [7] were used as discriminants:

- dE/dx , as measured in the CTD;
- $E^{\text{CAL}}/p^{\text{track}}$, the energy of the EFO as measured in the calorimeter, divided by the track momentum;
- d_{cell} , the depth of the central energy deposit within the CAL.

The following discriminating variables were used to distinguish the origin of electron candidates:

- p_T^{rel} , the transverse-momentum component of the electron candidate relative to the direction of the jet axis. The shapes of the light-quark p_T^{rel} distributions in the MC were corrected [42] using a background-enriched data sample. This variable is sensitive to b decays since electrons from b decays tend to have large p_T^{rel} due to the large b mass;
- $\Delta\phi$, the difference of azimuthal angles of the electron candidate and the missing trans-

verse momentum vector, defined as

$$\Delta\phi = |\phi(\vec{p}_e) - \phi(\vec{\not{p}}_T)|,$$

where $\vec{\not{p}}_T$ is the negative vector sum of the EFO momentum transverse to the beam axis,

$$\vec{\not{p}}_T = -(\sum_i p_x^i, \sum_i p_y^i),$$

and the sum runs over all EFOs. The variable $\Delta\phi$ is sensitive to semileptonic decays of b and c hadrons due to the presence of the neutrino;

- $d/\delta d$, the signed decay-length significance, where δd is the uncertainty on d [48, 50]. This variable is sensitive to the decay of c and b hadrons due to their long lifetimes.

In contrast to the results of a previous ZEUS study [7], the separation power of $\Delta\phi$ and p_T^{rel} is worse due to the lower jet momenta used here. Therefore it was not possible to separate the charm signal from the other particles in the electron background.

Following the procedure of the previous study [7], the six variables were combined into one discriminating test-function variable, which is a ratio of likelihoods. For a given hypothesis of particle, i , and source j , the likelihood, \mathcal{L}_{ij} , is given by

$$\mathcal{L}_{ij} = \prod_l \mathcal{P}_{ij}(d_l),$$

where $\mathcal{P}_{ij}(d_l)$ is the probability to observe particle i from source j with value d_l of a discriminant variable. The particle hypotheses $i \in \{e, \pi, K, p\}$ and the sources, $j \in \{b \rightarrow e, \text{other } e, \text{non-}e\}$, were considered. For the likelihood ratio test, the test function T_{ij} was defined as

$$T_{ij} = \frac{\alpha_i \alpha'_j \mathcal{L}_{ij}}{\sum_{k,l} \alpha_k \alpha'_l \mathcal{L}_{kl}}.$$

The α_i, α'_j denote the prior probabilities taken from MC. In the sum, k, l run over all particle types and sources defined above. In the following, T is always taken to be the likelihood ratio for an electron originating from a semileptonic b -quark decay, $T \equiv T_{e,b \rightarrow e}$, unless otherwise stated.

7 Signal extraction

The combined MC sample was split into the three contributions as defined in the previous section. The beauty test function, T , was calculated separately for these three samples and for the data. The relative contributions of the three sources in the data, $f_{b \rightarrow e}^{\text{DATA}}$, $f_{\text{other } e}^{\text{DATA}}$, $f_{\text{non-}e}^{\text{DATA}}$, were obtained from a three-component maximum-likelihood fit [51] to the

T distributions. The fit range of the test function was restricted to $-2 \ln T < 10$ to remove the region dominated by background and where the test function falls rapidly. The χ^2 for the fit is $\chi^2/\text{ndf} = 18/28$.

The result of the fit is shown in Fig. 2 and corresponds to a scaling of the cross section predicted by the beauty MC by a factor of 1.32 ± 0.11 . For the other two samples the scaling factors were determined to be ~ 1.1 for the electron background and ~ 1.3 for the non- e background. These factors were applied to the contributions shown in Figs. 3 and 4.

Figure 3 shows a comparison of the MC simulation to the data for the main variables used for the event selection. The Monte Carlo describes the data well. Figure 4 shows the distributions for the variables in the likelihood-ratio test function, which are sensitive to the different origin of the electron candidates. In Figs. 4 (a), (c) and (e), the three variables are shown for the selection used in the fit. Figures 4 (b), (d) and (f), show the same distributions for a signal-enriched region, which is defined by a harder cut on the test function at $-2 \ln T < 1.5$. All distributions are reasonably well described.

8 Cross-section determination

The differential beauty cross section for a variable, v , was determined separately for each bin, k , from the relative fractions in the data obtained from the fit and the acceptance correction, $\mathcal{A}_{b \rightarrow e}^{v_k}$, calculated using MC events,

$$\frac{d\sigma_{b \rightarrow e}}{dv_k} = \frac{N^{\text{DATA}} \cdot f_{b \rightarrow e}^{\text{DATA}}(v_k)}{\mathcal{A}_{b \rightarrow e}^{v_k} \cdot \mathcal{L} \cdot \Delta v_k} \cdot C_r, \quad (1)$$

where N^{DATA} is the number of electron candidates found in the data bin, \mathcal{L} is the integrated luminosity, Δv_k is the bin width and C_r is the QED radiative-correction factor. The acceptance is defined as

$$\mathcal{A}_{b \rightarrow e} = \frac{N_{b \rightarrow e}^{\text{rec}}}{N_{b \rightarrow e}^{\text{true}}},$$

where $N_{b \rightarrow e}^{\text{rec}}$ is the number of electrons from semileptonic decays reconstructed in the MC sample satisfying the selection criteria detailed in Section 5, and $N_{b \rightarrow e}^{\text{true}}$ is the number of electrons from semileptonic decays produced in the signal process that satisfy the kinematic requirements of the cross-section definition using the MC information at the generator level. The kinematic variables Q^2 and x at the true level were calculated using the four-momentum of the exchanged photon after possible initial-state radiation (ISR).

The cross sections were corrected to the QED Born level, calculated using a running coupling constant, α_{em} , such that they can be compared directly to the NLO QCD predictions by HVQDIS. The radiative corrections were obtained using the RAPGAP Monte Carlo as

$C_r = \sigma_{\text{Born}}/\sigma_{\text{rad}}$, where σ_{rad} is the cross section with full QED corrections (as used in the standard MC samples) and σ_{Born} was obtained with the QED corrections turned off. The corrections are typically $C_r \approx 1.05$ rising to $C_r \approx 1.10$ for the high Q^2 region.

9 Systematic uncertainties

The systematic uncertainties were calculated by varying the analysis procedure and then repeating the fit to the likelihood distributions [42]. The variations were made in a range such that the MC continued to provide a reasonable description of the data for the relevant distributions. The systematic uncertainties were determined bin by bin, unless stated otherwise. The main contributions came from the following sources, where the numbers in parentheses correspond to the uncertainty on the total cross section:

1. DIS selection – the preselection cuts on the scattered electron were varied in both data and MC. The only cuts that had a significant effect were the cut on the energy, which was varied between $9 < E_{e'} < 11$ GeV, the cut on the inelasticity, which was varied between $0.04 < y_{\text{JB}} < 0.06$, and the energy window for $E - p_z$, which was varied by ± 4 GeV ($^{+1.7\%}_{-1.5\%}$);
2. trigger efficiency – the uncertainty on the trigger efficiency was evaluated by comparing events taken with independent triggers (+1.2%);
3. dE/dx simulation – both the mean and the width of the dE/dx distribution were varied in the MC separately and simultaneously by the uncertainty estimated from the data [23]. These two variations were then combined, giving a conservative estimate of the uncertainty on the dE/dx test function ($^{+0.4\%}_{-0.4\%}$);
4. tracking efficiency – the track-finding inefficiency in the data with respect to the MC was estimated to be at most 2%. The overall uncertainty due to this tracking inefficiency was determined by randomly rejecting 2% of all tracks in the MC and repeating the secondary-vertex finding (−3.4%);
5. decay-length smearing – the fraction of events in the MC where the decay-length smearing was applied was varied by $\pm 2\%$ and the additional terms for the smearing of the tails were switched off ($^{+2.6\%}_{-2.0\%}$);
6. p_T^{rel} shape correction – the correction applied to the MC was switched off and increased by an additional 50% ($^{-1.5\%}_{-2.4\%}$);
7. electron background – the relative contributions of the different electron sources in the MC were changed by varying separately the contributions from photon conversions, Dalitz decays, semileptonic decays from charm and DIS electrons by $\pm 25\%$ ($^{+2.5\%}_{-2.4\%}$);

8. charm-spectrum reweighting – the correction to the c -decay electron spectrum in the MC using the CLEO data was varied by $\pm 50\%$ ($^{+3.4}_{-2.9}\%$);
9. energy scale – the global energy scale was varied in the MC by $\mp 2\%$ ($^{+1.2}_{-1.0}\%$);
10. jet energy scale – the calorimetric part of the transverse jet energy in MC was varied by $\pm 3\%$ ($^{+1.7}_{+0.7}\%$);
11. MC model dependence – the Q^2 reweighting correction was varied by a factor of two ($^{+2.0}_{-1.9}\%$);
12. electron reconstruction efficiency – the electron reconstruction efficiency in MC was varied by ± 0.05 in the FCAL and RCAL regions and by ∓ 0.05 in the BCAL region ($^{+4.0}_{-3.7}\%$).

A series of further checks were made. The fit range was varied to check possible deficits in the background description. Selection cuts such as the Z vertex position or preselection cuts such as on the dE/dx test function were varied before repeating the analysis. Another important check was the charge dependence. Separate fits were made for electron and positron candidates for each lepton-beam charge separately as well as for the combined sample. All variations were found to be small and consistent with the expected fluctuations due to statistics and were therefore not included in the systematic error.

The individual contributions to the systematic uncertainties were added in quadrature, separately for the negative and the positive variations, to determine the systematic uncertainty of $^{+7.4}_{-7.7}\%$ for the total cross section. A $\pm 2.0\%$ overall normalisation uncertainty associated with the luminosity measurement was included in the uncertainty on the total cross section.

10 Results

The visible cross section for electrons from direct and indirect b -quark decays with $0.9 < p_T^e < 8 \text{ GeV}$ in the range $|\eta^e| < 1.5$ was measured in DIS events with $Q^2 > 10 \text{ GeV}^2$ and $0.05 < y < 0.7$ and found to be

$$\sigma_{b \rightarrow e} = (71.8 \pm 5.5(\text{stat.})_{-5.5}^{+5.3}(\text{syst.})) \text{ pb.}$$

This cross section includes all electrons and positrons from both b and \bar{b} and no jet requirement was applied at the true level. This result can be compared to the HVQDIS NLO QCD prediction of

$$\sigma_{b \rightarrow e}^{\text{NLO}} = (67_{-11}^{+10}) \text{ pb,}$$

where the uncertainty is calculated as described in Section 4. This value agrees well with the measured cross section, which is a factor 1.3 higher than the RAPGAP leading-order prediction³ of 54.4 pb. This factor is used to scale the RAPGAP predictions in Figs. 5 and 6.

Differential cross sections as a function of p_T^e and η_e , Q^2 and x are shown in Fig. 5. Figure 6 shows the differential cross sections as a function of x , split into four different Q^2 ranges. The figures also show the NLO QCD and the scaled RAPGAP predictions. The cross-section values are given in Tables 1–3. Both the predictions from the NLO QCD calculations as well as the scaled RAPGAP cross sections describe the data well.

11 Extraction of $F_2^{b\bar{b}}$

The structure function $F_2^{b\bar{b}}$ can be defined in terms of the inclusive double-differential cross section (defined in analogy to Eq. 1) as a function of x and Q^2 ,

$$\frac{d^2\sigma_{b\bar{b}}}{dx dQ^2} = \frac{Y_+(2\pi\alpha_{\text{em}}^2)}{xQ^4} \left[F_2^{b\bar{b}}(x, Q^2) - \frac{y^2}{Y_+} F_L^{b\bar{b}}(x, Q^2) \right],$$

where $Y_+ = 1 + (1 - y)^2$ and $F_L^{b\bar{b}}$ is the beauty contribution to the structure function F_L . The electron cross section, $\sigma_{b \rightarrow e}$, measured in bins of x and Q^2 , was used to extract $F_2^{b\bar{b}}$ at a reference point in the x - Q^2 plane using

$$F_2^{b\bar{b}}(x, Q^2) = \frac{d^2\sigma_{b \rightarrow e}}{dx dQ^2} \cdot \frac{F_2^{b\bar{b},\text{NLO}}(x, Q^2)}{d^2\sigma_{b \rightarrow e}^{\text{NLO}}/dx dQ^2},$$

where $F_2^{b\bar{b},\text{NLO}}$ and $d^2\sigma_{b \rightarrow e}^{\text{NLO}}/dx dQ^2$ were calculated in the FFNS using the HVQDIS program. The uncertainty on the extrapolation from the measured range to the full kinematic phase space was estimated by varying the settings of the calculation (see Section 4) for $F_2^{b\bar{b},\text{NLO}}/(d^2\sigma_{b \rightarrow e}^{\text{NLO}}/dx dQ^2)$ and adding the resulting uncertainties in quadrature. For each bin, a reference point in x and Q^2 was defined (see Table 4) to calculate the structure function. The small correction for $F_L^{b\bar{b}}$ is taken into account in the HVQDIS prediction.

The structure function $F_2^{b\bar{b}}$ is shown in Fig. 7 as a function of x for nine different values of Q^2 . The values and the corresponding uncertainties are given in Table 4. To compare the result with previous measurements [3, 4, 12], the earlier results were extrapolated to the Q^2 values chosen in this analysis. For $Q^2 > 10 \text{ GeV}^2$, this measurement represents the most precise determination of $F_2^{b\bar{b}}$ by the ZEUS Collaboration. It is in good agreement with previous ZEUS analyses and the H1 measurement. The NLO QCD prediction

³ Note that the RAPGAP predictions do not include the Q^2 reweighting correction discussed in Section 3.

describes the data well. The same measurements are also shown as a function of Q^2 for fixed x in Fig. 8, compared to several NLO and NNLO QCD predictions based on the fixed- or variable-flavour-number schemes [52]. For the HVQDIS prediction shown in this figure, the scale parametrisation $\mu = \frac{1}{2}\sqrt{Q^2 + p_T^2 + m_b^2}$ [3], was used. All the theoretical predictions shown provide a good description of the data.

12 Conclusions

Beauty production has been measured in DIS using semileptonic decays into electrons. A likelihood-ratio test function, adapted from a previous measurement, was used to identify the signal. The analysis benefited from the improved tracking in the HERA II data-set through the use of the measured decay length of weakly decaying B hadrons.

The total cross section and differential cross sections as a function of x , Q^2 , p_T^e and η^e were determined. NLO QCD predictions calculated using the HVQDIS program describe the data well. The RAPGAP Monte Carlo provides a good description of the shape of the differential distributions.

The structure function $F_2^{b\bar{b}}$ was extracted from the double-differential cross section as a function of x and Q^2 . The measurement is in agreement with the results obtained from previous analyses using different techniques. For $Q^2 > 10 \text{ GeV}^2$, this measurement represents the most precise determination of $F_2^{b\bar{b}}$ by the ZEUS Collaboration. The results were also compared to several NLO and NNLO QCD calculations, which provide a good description of the data.

Acknowledgements

It is a pleasure to thank the ABKM, CTEQ, GJR and MRST groups that provided the predictions for $F_2^{b\bar{b}}$ shown in Fig. 8. We appreciate the contributions to the construction and maintenance of the ZEUS detector of many people who are not listed as authors. The HERA machine group and the DESY computing staff are especially acknowledged for their success in providing excellent operation of the collider and the data-analysis environment. We thank the DESY directorate for their strong support and encouragement.

References

- [1] E. Laenen et al., Nucl. Phys. **B 392**, 162 (1993).
- [2] E. Laenen et al., Nucl. Phys. **B 392**, 229 (1993).
- [3] ZEUS Collab., H. Abramowicz et. al., Eur. Phys. J. **C 69**, 347 (2010).
- [4] ZEUS Collab., S. Chekanov et. al., Eur. Phys. J. **C 65**, 65 (2010).
- [5] ZEUS Collab., S. Chekanov et. al., JHEP **04**, 133 (2009).
- [6] ZEUS Collab., S. Chekanov et. al., JHEP **02**, 032 (2009).
- [7] ZEUS Collab., S. Chekanov et. al., Phys. Rev. **D 78**, 072001 (2008).
- [8] ZEUS Collab., S. Chekanov et al., Eur. Phys. J. **C 50**, 1434 (2007).
- [9] ZEUS Collab., S. Chekanov et al., Phys. Lett. **B 599**, 173 (2004).
- [10] ZEUS Collab., S. Chekanov et al., Phys. Rev. **D 70**, 12008 (2004). Erratum-ibid **D 74**, 59906 (2006).
- [11] ZEUS Collab., J. Breitweg et al., Eur. Phys. J. **C 18**, 625 (2001).
- [12] H1 Collab. F.D. Aaron et al., Eur. Phys. J. **C 65**, 89 (2010).
- [13] H1 Collab., A. Aktas et al., Eur. Phys. J. **C 47**, 597 (2006).
- [14] H1 Collab., A. Aktas et al., Eur. Phys. J. **C 45**, 23 (2006).
- [15] H1 Collab., A. Aktas et al., Phys. Lett. **B 621**, 56 (2005).
- [16] H1 Collab., A. Aktas et al., Eur. Phys. J. **C 40**, 349 (2005).
- [17] H1 Collab., A. Aktas et al., Eur. Phys. J. **C 41**, 453 (2005).
- [18] H1 Collab., C. Adloff et al., Phys. Lett. **B 467**, 156 (1999).
- [19] ZEUS Collab., U. Holm (ed.), *The ZEUS Detector*. Status Report (unpublished), DESY (1993), available on <http://www-zeus.desy.de/bluebook/bluebook.html>.
- [20] N. Harnew et al., Nucl. Instr. and Meth. **A 279**, 290 (1989);
B. Foster et al., Nucl. Phys. Proc. Suppl. **B 32**, 181 (1993);
B. Foster et al., Nucl. Instr. and Meth. **A 338**, 254 (1994).
- [21] A. Polini et al., Nucl. Instr. and Meth. **A 581**, 656 (2007).
- [22] ZEUS Collab., J. Breitweg et al., Phys. Lett. **B 481**, 213 (2000).
- [23] D. Bartsch, Ph.D. Thesis, Universität Bonn, Bonn, Germany, Report BONN-IR-2007-05, 2007, available on http://brock.physik.uni-bonn.de/zeus_pub.php.

- [24] M. Derrick et al., Nucl. Instr. and Meth. **A 309**, 77 (1991);
A. Andresen et al., Nucl. Instr. and Meth. **A 309**, 101 (1991);
A. Caldwell et al., Nucl. Instr. and Meth. **A 321**, 356 (1992);
A. Bernstein et al., Nucl. Instr. and Meth. **A 336**, 23 (1993).
- [25] J. Andruszków et al., Preprint DESY-92-066, DESY, 1992;
ZEUS Collab., M. Derrick et al., Z. Phys. **C 63**, 391 (1994);
J. Andruszków et al., Acta Phys. Pol. **B 32**, 2025 (2001).
- [26] M. Helbich et al., Nucl. Instr. and Meth. **A 565**, 572 (2006).
- [27] H. Jung, Comp. Phys. Comm. **86**, 147 (1995). See also
<http://projects.hepforge.org/rapgap/>.
- [28] CTEQ Collab., H.L. Lai et al., Eur. Phys. J. **C 12**, 375 (2000).
- [29] A. Kwiatkowski, H. Spiesberger and H.-J. Möhring, Comp. Phys. Comm.
69, 155 (1992). Also in *Proc. Workshop Physics at HERA*, eds. W. Buchmüller and
G. Ingelman, (DESY, Hamburg, 1991).
- [30] G.A. Schuler and H. Spiesberger, *Proc. Workshop on Physics at HERA*,
W. Buchmüller and G. Ingelman (eds.), Vol. 3, p. 1419. Hamburg, Germany, DESY
(1991).
- [31] L. Lönnblad, Comp. Phys. Comm. **71**, 15 (1992).
- [32] Particle Data Group, C. AMSLER et al., Phys. Lett. **B 667**, 1 (2008).
- [33] T. Sjöstrand, Comp. Phys. Comm. **82**, 74 (1994);
T. Sjöstrand et al., Comp. Phys. Comm. **135**, 238 (2001).
- [34] CLEO Collaboration, N.E. Adam et al., Phys. Rev. Lett. **97**, 251801 (2006).
- [35] R. Brun et al., GEANT3, Technical Report CERN-DD/EE/84-1, CERN, 1987.
- [36] B.W. Harris and J. Smith, Phys. Rev. **D 57**, 2806 (1998).
- [37] J. Smith and W.L. van Neerven, Nucl. Phys. **B 374**, 36 (1992).
- [38] ZEUS Collab., S. Chekanov et al., Phys. Rev. **D 67**, 012007 (2003).
- [39] C. Peterson et al., Phys. Rev. **D 27**, 105 (1983).
- [40] P. Nason and C. Oleari, Nucl. Phys. **B 565**, 245 (2000).
- [41] W.H. Smith, K. Tokushuku and L.W. Wiggers, *Proc. Computing in High-Energy
Physics (CHEP), Annecy, France*, C. Verkerk and W. Wojcik (eds.), p. 222.
CERN, Geneva, Switzerland (1992). Also in preprint DESY 92-150B.
- [42] R. Shehzadi, Ph.D. Thesis, Universität Bonn, Bonn, Germany, Report
BONN-IR-11-01, 2011, available on
http://brock.physik.uni-bonn.de/zeus_pub.php.

- [43] ZEUS Collab., J. Breitweg et al., *Eur. Phys. J.* **C 1**, 81 (1998);
G.M. Briskin, Ph.D. Thesis, Tel Aviv University, Report DESY-THESIS 1998-036, 1998.
- [44] S.D. Ellis and D.E. Soper, *Phys. Rev.* **D 48**, 3160 (1993).
- [45] S. Catani et al., *Nucl. Phys.* **B 406**, 187 (1993).
- [46] S. Bentvelsen, J. Engelen and P. Kooijman, *Proc. Workshop on Physics at HERA*, W. Buchmüller and G. Ingelman (eds.), Vol. 1, p. 23. Hamburg, Germany, DESY (1992).
- [47] F. Jacquet and A. Blondel, *Proceedings of the Study for an ep Facility for Europe*, U. Amaldi (ed.), p. 391. Hamburg, Germany (1979). Also in preprint DESY 79/48.
- [48] V. Schönberg, Ph.D. Thesis, Universität Bonn, Bonn, Germany, Report BONN-IR-10-05, 2010, available on http://brock.physik.uni-bonn.de/zeus_pub.php.
- [49] M. Jüngst, Ph.D. Thesis, Universität Bonn, Bonn, Germany, Report BONN-IR-10-03, 2010, available on http://brock.physik.uni-bonn.de/zeus_pub.php.
- [50] A.G. Yagües Molina, Ph.D. Thesis, Humboldt University, Berlin, Germany, Report ID:6561, 2008.
- [51] R. Barlow and C. Beeston, *Comp. Phys. Comm.* **77**, 219 (1993).
- [52] P.M. Nadolsky et al., *Phys. Rev.* **D 78**, 013004 (2008);
A.D. Martin et al., *Eur. Phys. J.* **C 63**, 189 (2009);
R.S. Thorne, and W.K. Tung, Preprint arXiv:0809.0714, 2008;
M. Glück, P. Jimenez-Delgado and E. Reya, *Eur. Phys. J.* **C 53**, 355 (2008);
S. Alekhin and S. Moch, *Phys. Lett.* **B 672**, 166 (2009);
S. Alekhin et al., *Phys. Rev.* **D 81**, 014032 (2010);
S. Alekhin, J. Blumlein, S. Moch, *PoS DIS2010*, 021 (2010).

Q^2 (GeV ²)	$d\sigma_{b\rightarrow e}/dQ^2$ (pb/GeV ²)	$d\sigma_{b\rightarrow e}^{\text{NLO}}/dQ^2$ (pb/GeV ²)
10 : 20	$1.73\pm 0.40^{+0.20}_{-0.29}$	$1.93^{+0.37}_{-0.37}$
20 : 40	$1.05\pm 0.18^{+0.12}_{-0.07}$	$0.84^{+0.13}_{-0.15}$
40 : 80	$0.428\pm 0.063^{+0.036}_{-0.037}$	$0.327^{+0.050}_{-0.057}$
80 : 200	$0.070\pm 0.015^{+0.006}_{-0.014}$	$0.087^{+0.011}_{-0.013}$
200 : 1000	$0.0057\pm 0.0014^{+0.0003}_{-0.0010}$	$0.0066^{+0.0006}_{-0.0007}$

x	$d\sigma_{b\rightarrow e}/dx$ (pb)	$d\sigma_{b\rightarrow e}^{\text{NLO}}/dx$ (pb)
0.0002 : 0.0010	$34800\pm 5700^{+5400}_{-7300}$	29700^{+5400}_{-6100}
0.0010 : 0.0020	$19400\pm 2700^{+1900}_{-1900}$	14700^{+2400}_{-2800}
0.0020 : 0.0040	$5800\pm 1100^{+600}_{-400}$	5900^{+900}_{-1100}
0.0040 : 0.0100	$1200\pm 310^{+210}_{-220}$	1560^{+220}_{-230}
0.0100 : 0.1000	$38.4\pm 12.1^{+9.7}_{-8.7}$	$48.5^{+6.2}_{-5.7}$

Table 1: *Differential cross sections for electrons from b-quark decays as a function of Q^2 and x . The cross sections are given for $Q^2 > 10 \text{ GeV}^2$, $0.05 < y < 0.7$, $0.9 < p_T^e < 8 \text{ GeV}$ and $|\eta^e| < 1.5$. The first uncertainty is statistical and the second is systematic. In addition, the NLO QCD prediction and its uncertainty are given.*

p_T^e (GeV)	$d\sigma_{b \rightarrow e}/dp_T^e$ (pb/GeV)	$d\sigma_{b \rightarrow e}^{\text{NLO}}/dp_T^e$ (pb/GeV)
0.9 : 2.1	$36.9 \pm 6.1^{+4.2}_{-5.7}$	$33.1^{+6.1}_{-6.3}$
2.1 : 3.2	$12.2 \pm 2.0^{+1.7}_{-0.8}$	$12.0^{+1.8}_{-2.0}$
3.2 : 4.5	$3.08 \pm 0.90^{+0.60}_{-0.44}$	$4.36^{+0.59}_{-0.67}$
4.5 : 8.0	$0.78 \pm 0.20^{+0.16}_{-0.18}$	$0.95^{+0.13}_{-0.12}$

η^e	$d\sigma_{b \rightarrow e}/d\eta^e$ (pb)	$d\sigma_{b \rightarrow e}^{\text{NLO}}/d\eta^e$ (pb)
-1.5 : -0.5	$15.1 \pm 3.7^{+2.7}_{-2.0}$	$13.4^{+2.3}_{-2.7}$
-0.5 : 0.0	$26.0 \pm 3.8^{+3.7}_{-3.6}$	$26.7^{+4.3}_{-5.1}$
0.0 : 0.5	$30.3 \pm 5.1^{+4.4}_{-5.3}$	$30.0^{+4.7}_{-5.6}$
0.5 : 1.5	$28.6 \pm 3.7^{+1.7}_{-3.6}$	$23.2^{+3.9}_{-3.9}$

Table 2: Differential cross sections for electrons from b -quark decays as a function of p_T^e and η^e . The cross sections are given for $Q^2 > 10 \text{ GeV}^2$, $0.05 < y < 0.7$, $0.9 < p_T^e < 8 \text{ GeV}$ and $|\eta^e| < 1.5$. The first uncertainty is statistical and the second is systematic. In addition, the NLO QCD prediction and its uncertainty are given.

Q^2 (GeV ²)	x	$d^2\sigma_{b \rightarrow e}/dx dQ^2$ (pb/GeV ²)	$d^2\sigma_{b \rightarrow e}^{\text{NLO}}/dx dQ^2$ (pb/GeV ²)
10 : 20	0.0001 : 0.0004	$2700 \pm 1200^{+300}_{-700}$	2500^{+400}_{-500}
10 : 20	0.0004 : 0.0030	$300 \pm 100^{+40}_{-80}$	480^{+100}_{-100}
20 : 60	0.0003 : 0.0012	$477 \pm 84^{+47}_{-60}$	343^{+525}_{-650}
20 : 60	0.0012 : 0.0020	$239 \pm 51^{+47}_{-36}$	180^{+300}_{-325}
20 : 60	0.0020 : 0.0060	$36 \pm 12^{+15}_{-14}$	42^{+8}_{-8}
60 : 400	0.0009 : 0.0035	$9.6 \pm 2.0^{+1.9}_{-1.6}$	$8.9^{+1.0}_{-1.3}$
60 : 400	0.0035 : 0.0070	$3.6 \pm 1.3^{+1.0}_{-0.6}$	$5.0^{+0.6}_{-0.7}$
60 : 400	0.0070 : 0.0400	$0.23 \pm 0.12^{+0.06}_{-0.13}$	$0.47^{+0.06}_{-0.06}$
400 : 1000	0.0050 : 0.1000	$0.013 \pm 0.010^{+0.009}_{-0.007}$	$0.029^{+0.002}_{-0.003}$

Table 3: Double-differential cross sections for electrons from b -quark decays as a function of x for four different Q^2 ranges. The cross sections are given for $Q^2 > 10 \text{ GeV}^2$, $0.05 < y < 0.7$, $0.9 < p_T^e < 8 \text{ GeV}$ and $|\eta^e| < 1.5$. The first uncertainty is statistical and the second is systematic. In addition, the NLO QCD prediction and its uncertainty are given.

Q^2 (GeV)	x	$F_2^{b\bar{b}}$
12	0.0002	0.0074 ± 0.0033 ^{+0.0010 +0.0012} _{-0.0020 -0.0015}
15	0.0013	0.0021 ± 0.0007 ^{+0.0003 +0.0004} _{-0.0005 -0.0004}
25	0.0005	0.0152 ± 0.0027 ^{+0.0015 +0.0025} _{-0.0019 -0.0029}
30	0.0013	0.0110 ± 0.0023 ^{+0.0022 +0.0019} _{-0.0017 -0.0021}
40	0.005	0.0041 ± 0.0014 ^{+0.0017 +0.0009} _{-0.0016 -0.0007}
80	0.002	0.0208 ± 0.0043 ^{+0.0041 +0.0029} _{-0.0036 -0.0032}
120	0.005	0.0110 ± 0.0040 ^{+0.0029 +0.0015} _{-0.0019 -0.0015}
180	0.013	0.0050 ± 0.0027 ^{+0.0014 +0.0006} _{-0.0027 -0.0006}
600	0.013	0.0089 ± 0.0067 ^{+0.0057 +0.0008} _{-0.0048 -0.0008}

Table 4: The structure function $F_2^{b\bar{b}}$ given for nine different values of Q^2 and x . The first error is statistical, the second systematic and the last is the extrapolation uncertainty.

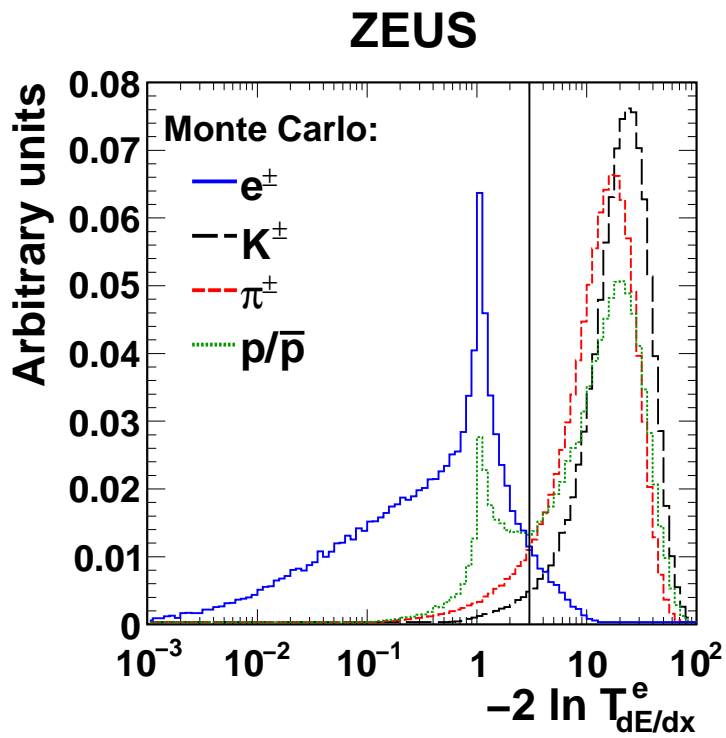


Figure 1: Distribution of the likelihood-ratio test function for the electron hypothesis, $T_{dE/dx}^e$, for e^\pm , π^\pm , K^\pm , p and \bar{p} . All histograms were normalised to unity. The selection cut at $-2 \ln T_{dE/dx}^e < 3$ is indicated by the vertical line. All other selection cuts were applied.

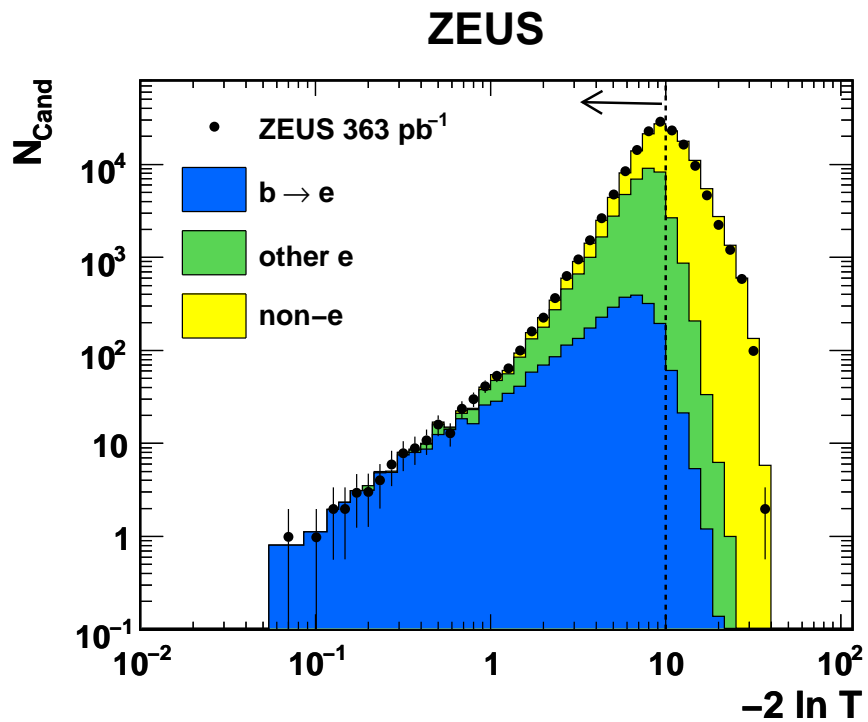


Figure 2: *The distribution of $-2 \ln T$, where T is the test function, using the beauty hypothesis for electron candidates, compared to the Monte Carlo expectation after the fit described in the text. The arrow indicates the region included in the fit ($-2 \ln T < 10$). The shaded areas show the fitted contributions for electrons from b -quark decays, electrons from other sources and the non-electron background.*

ZEUS

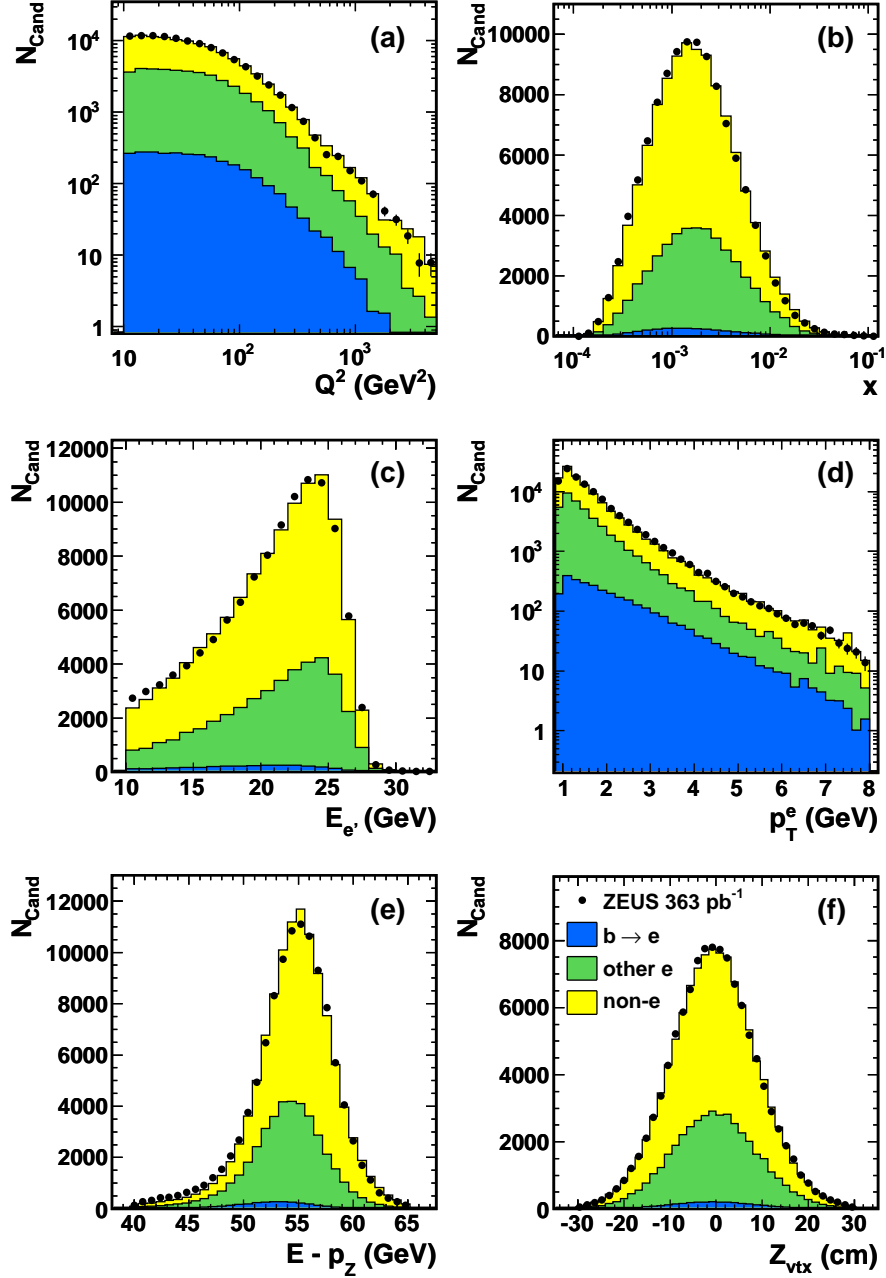


Figure 3: Distributions of the variables related to the event selection, after applying all selection cuts: for the kinematic variables (a) Q^2 and (b) x , for (c) the energy of the scattered electron, $E_{e'}$ and (d) the transverse momentum of the electron candidate, p_T^e . The variables $E - p_z$ and Z_{vtx} , which were used for the event selection are shown in (e) and (f), respectively. The shaded areas show the MC expectations for the contributions for electrons from b -quark decays, electrons from other sources and the non-electron background as denoted in the figure, after applying the scale factors from the fit. The summed distribution is compared with the data distribution shown by the black points.

ZEUS

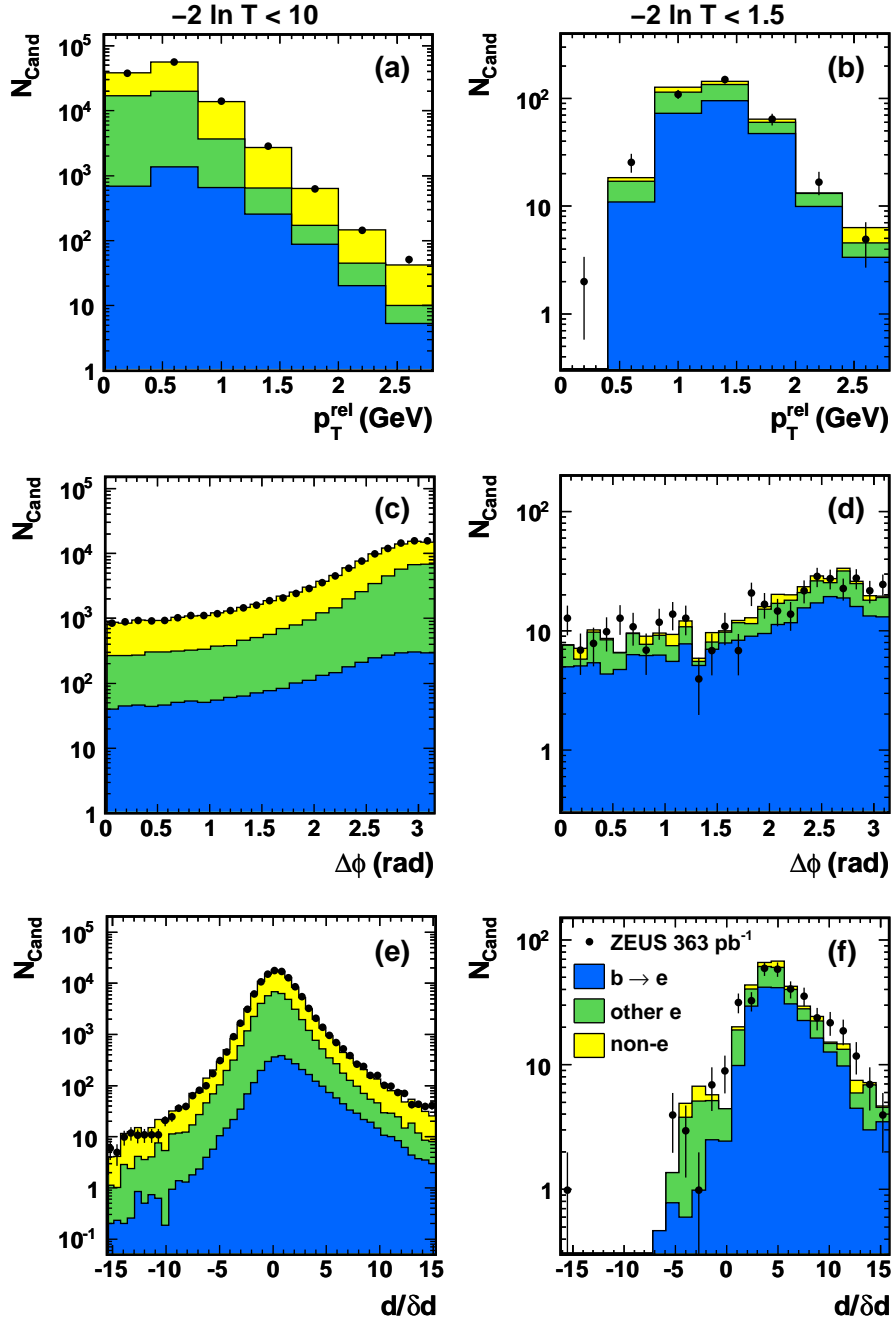


Figure 4: Distributions of (a) p_T^{rel} , (c) $\Delta\phi$ and (e) $d/\delta d$ for all candidates that enter the fit satisfying $-2\ln T < 10$. The same plots are shown for the beauty-enriched region ($-2\ln T < 1.5$) in (b), (d) and (f). For details see the caption of Fig. 3.

ZEUS

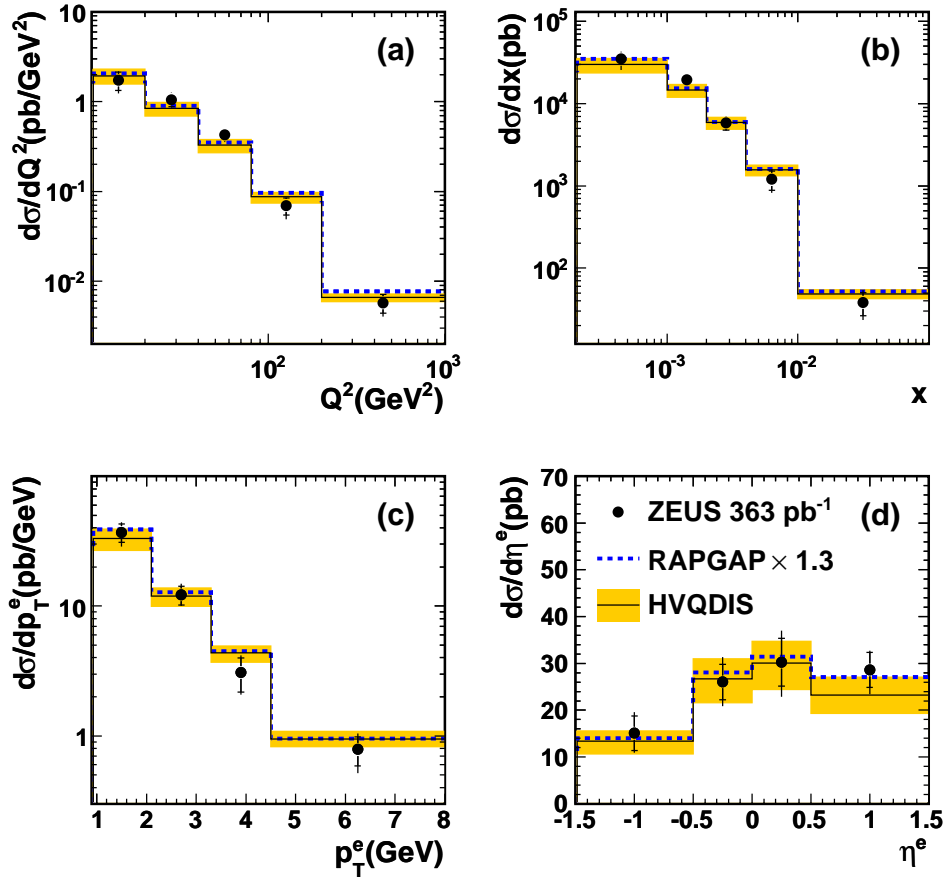


Figure 5: *Differential cross sections for electrons from b -quark decays as a function of the kinematic variables (a) Q^2 and (b) x , and the decay electron variables (c) p_T^e and (d) η^e . The cross sections are given for $Q^2 > 10 \text{ GeV}^2$, $0.05 < y < 0.7$, $0.9 < p_T^e < 8 \text{ GeV}$ and $|\eta^e| < 1.5$. The measurements are shown as points. The inner error bar shows the statistical uncertainty and the outer error bar shows the statistical and systematic uncertainties added in quadrature. The solid line shows the NLO QCD prediction, with the uncertainties indicated by the band; the dashed line shows the scaled prediction from RAPGAP.*

ZEUS

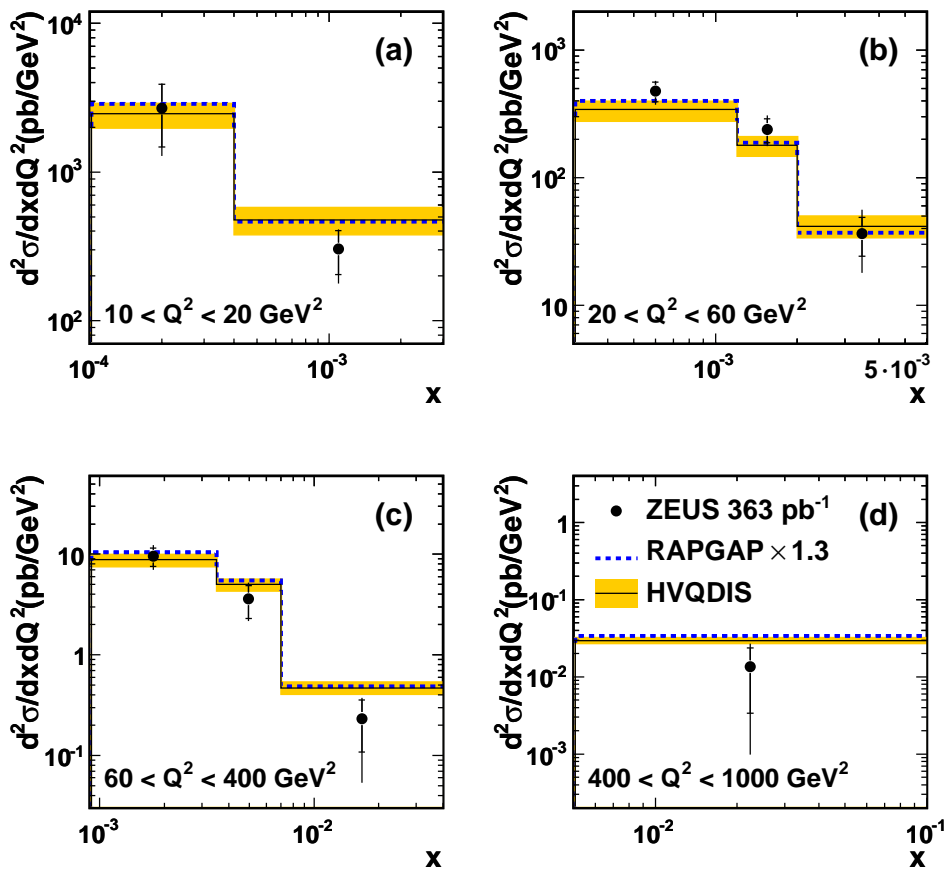


Figure 6: Double-differential cross sections for electrons from b -quark decays as a function of x for different regions of Q^2 . Other details as in the caption of Fig. 5.

ZEUS

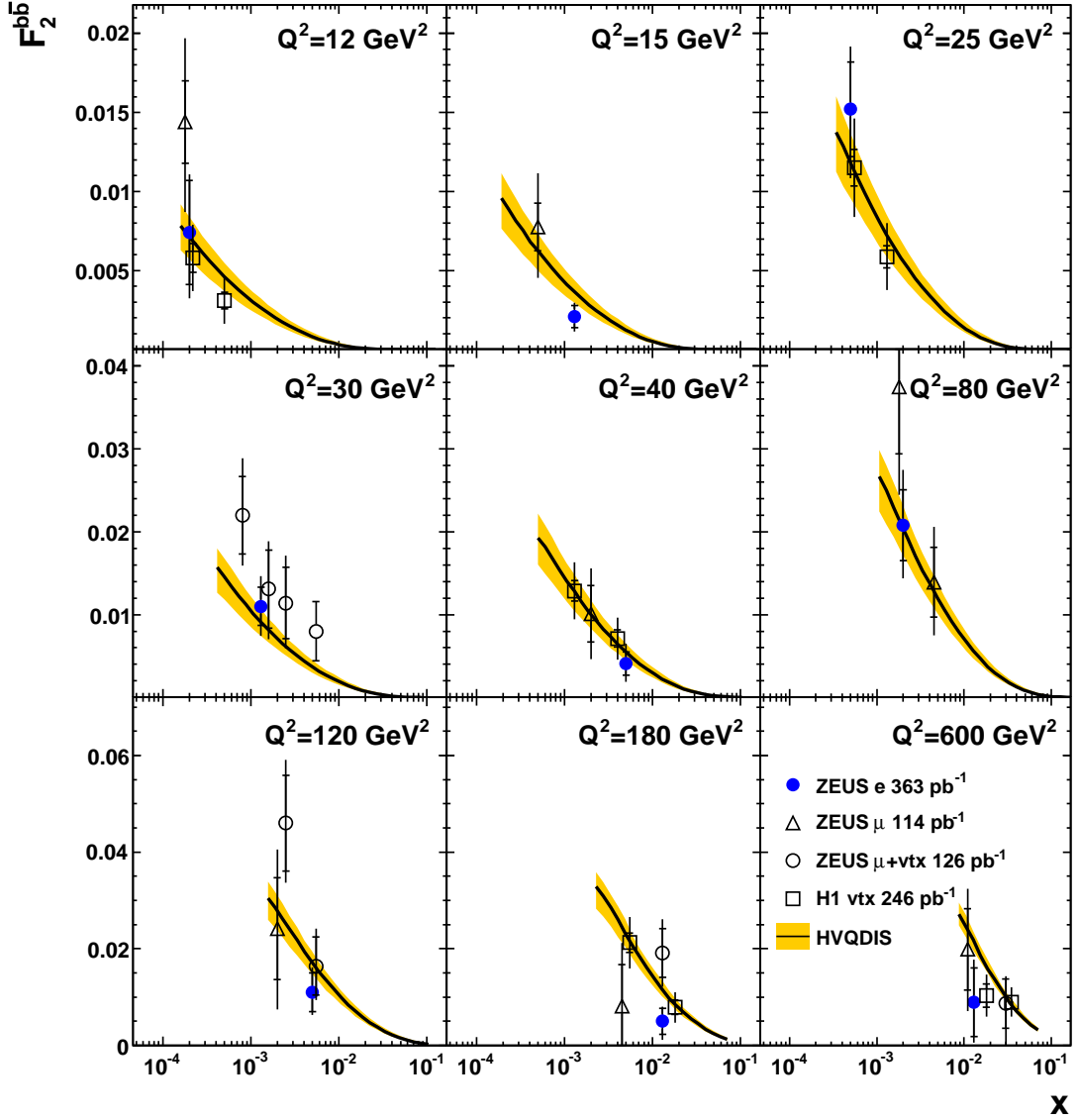


Figure 7: The structure function F_2^{bb} (filled symbols) as a function of x for nine different values of Q^2 compared to previous results (open symbols). The inner error bars are the statistical uncertainty while the outer error bars represent the statistical, systematic and extrapolation uncertainties added in quadrature. The band represents the uncertainty on the NLO QCD prediction. Previous data have been corrected to the reference Q^2 range of this analysis.

ZEUS

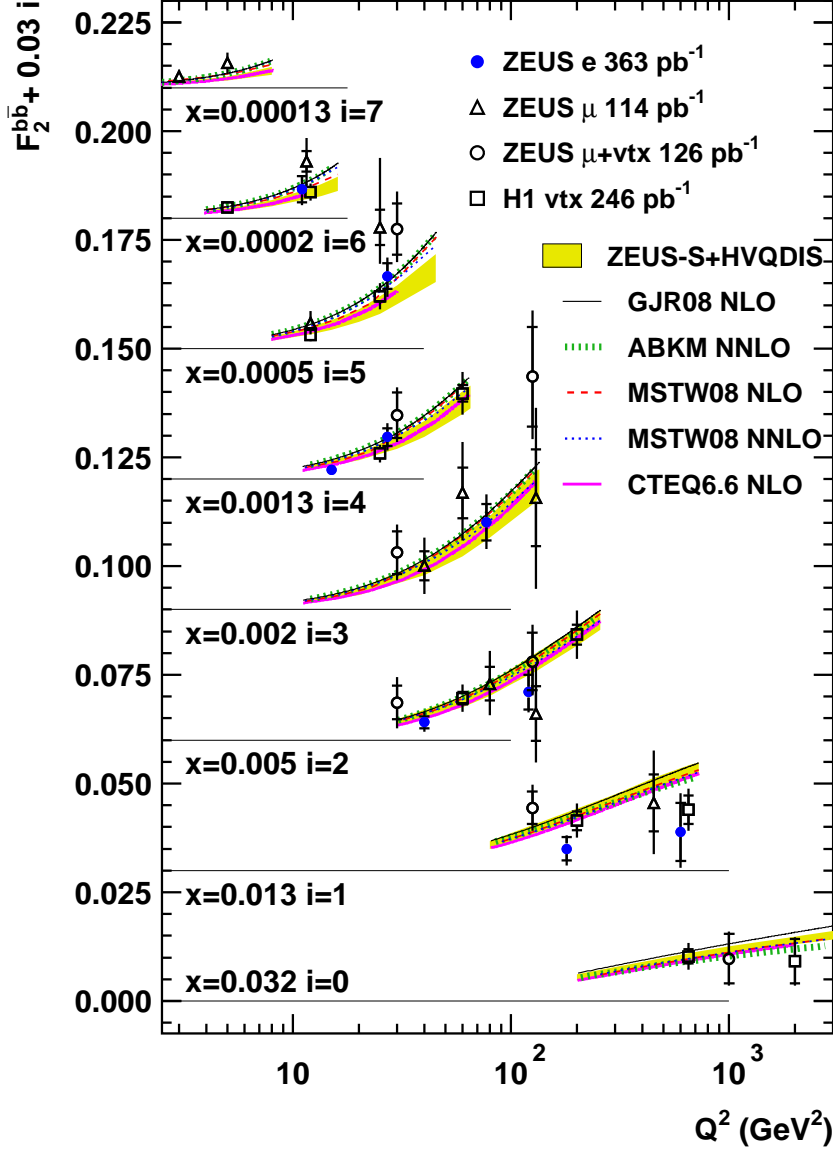


Figure 8: The structure function $F_2^{b\bar{b}}$ (filled symbols) as a function of Q^2 for fixed values of x compared to previous results (open symbols). The inner error bars are the statistical uncertainty while the outer error bars represent the statistical, systematic and extrapolation uncertainties added in quadrature. The data have been corrected to the same reference x as the previous analysis [3]. The measurements are compared to several NLO and NNLO QCD predictions (see text for details).